3112

Solar Energy Vol. 33, No. 3/4, pp. 253–264, 1984
Printed in the U.S.A.

0038–092X/84 $3.00 + .00

FREE CONVECTIVE TURBULENT FLOW WITHIN THE TROMBE WALL CHANNEL

T. R. Borgers† and H. Akbari
Lawrence Berkeley Laboratory, Berkeley CA 94720, U.S.A.

(*Received* 27 *April* 1979; *revision received* 20 *October* 1983; *accepted* 31 *October* 1983)

Abstract—A study of free convective turbulent heat transfer between parallel plates has been made. The initial flow is assumed to remain laminar until a combination of geometry, temperature, and flow rate conditions reach a pre-defined level. At this point the model used in this study assumes transition and permits laminar flow to gradually develop into fully turbulent flow. Turbulent flow characteristics are predicted by a mixing length model which incorporates empirical parameters used in the literature. Using air as the fluid, a wide range of channel geometries, relative surface temperatures, and flow rates have been examined. Guided by the very limited available experimental data, computations were made and several correlations were developed to enable important quantities to be estimated given the channel geometry, surface temperatures, and inlet air temperature.

1. INTRODUCTION

Free convective turbulent flow between heated parallel vertical plates has received little analytic attention in the past. Because of its application to passive solar thermocirculation systems, more information is needed. This work is intended to expand the scope of a previous study which dealt with laminar flow between heated parallel vertical plates[1]. The background material discussed in that reference will be omitted here.

A literature search reveals studies on free convective turbulent flow along a single heated vertical plate by Eckert and Jackson[2], Cheesewright[3], Warner and Arpaci[4], Kato *et al.*[5], Mason and Seban[6], Cebeci and Khattab[7], and Vliet and Liu[8]. Consistent experimental data is very difficult to obtain. Unsettling differences frequently appear whenever comparisons of results are made. Discussions of such differences are found in[6, 7]. No experimental studies of the problem stated here are known to the authors; hence relevant results of confined forced flow such as those of Hatton *et al.*[9] and Kays and Leung[10] have been used to provide guidelines for this study at the higher naturally induced flow rates. The studies noted by Refs. [3–8] have been helpful at the lower flow rates.

2. THEORY

The geometry of the model used in this study consists of two parallel, infinitely wide vertical plates, perfectly insulated on the outside with their bases in contact with a calm fluid at temperature T_0. The temperatures of the plates are constant and uniform at values T_g and T_w, both of which are greater than T_0 (Fig. 1).

The overall formulations remain identical to those described in[1], except for the introduction of approapriate terms which permit the gradual development of fully turbulent flow. Fluid flow at the channel entrance is assumed to be laminar. An estimate of the conditions at which turbulence is initiated is made. Thereafter, the development of turbulence is described by a modified mixing length model which incorporates a variable turbulent Prandtl number.

The transition point from laminar to turbulent flow has been examined experimentally for a single heated vertical plate in air by Cheesewright[3] and Warner and Arpaci[4]; in water by Lock and Trotter[11], Vliet and Liu[8], and by Godaux and Gebhart[12]. Reference is consistently made to the absence of a parameter which characterizes the beginning of transition to turbulent and fully turbulent flow adjacent to the vertical surface. A good discussion of the transition is provided by Godaux and Gebhart[12] who have observed that for a single heated surface, the thermal transition seems to depend upon the total amount of energy being convected locally in the boundary region at any elevation. For parallel plates at low volumetric

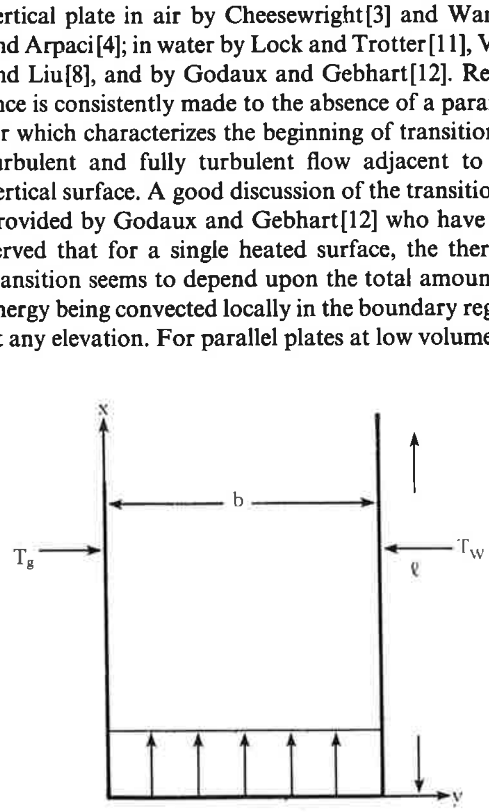

Fig. 1. Geometry of flow problem.

†Present address: Department of Chemistry, Humboldt State University, Arcata, CA 95521, U.S.A.

flow rates, the presence of one plate will have a negligible effect upon the behavior of the fluid adjacent to the other. However, at high volumetric flow rates, the presence of one plate affects the flow characteristics of the fluid adjacent to the other. The model used to describe this transition point must have the flexibility to account for either of these conditions. The experimental observations by Cheesewright[3] and Warner and Arpaci[4] for the single heated plate have shown that the transition point is adequately characterized by Grashof numbers. However, at higher channel flow rates the conditions for transition are expected to begin earlier and are assumed to be roughly proportional to Re^{-1}. The expression used to characterize the transition point is both Grashof and Reynolds number-dependent and is given by

$$Re(PrGr_x)^{1/3} = 4 \times 10^6. \tag{1}$$

This expression shows some similarity to the observations noted by Godaux and Gebhart[12] for a single plate and agrees quite well at low flow rates with the observations of Cheesewright[3] and Warner and Arpaci[4]. Valuable experimental work may be contributed toward characterization of the transition point for naturally induced convective channel flow. In this model, no provision is made to permit initiation of turbulence adjacent to one of the surfaces only. With reference to the laminar flow analysis[1], the continuity is unaltered

$$\frac{\partial u}{\partial x} + \frac{\partial v}{\partial y} = 0. \tag{2}$$

However, the momentum and energy equations become

$$u\frac{\partial u}{\partial x} + v\frac{\partial u}{\partial y} = \frac{1}{\rho}\frac{\partial}{\partial y}\left(u\frac{\partial u}{\partial y} - \rho\overline{u'v'}\right) - \frac{1}{\rho}\frac{\partial p}{\partial x} + g\beta(T - T_0) \tag{3}$$

$$u\frac{\partial T}{\partial x} + v\frac{\partial T}{\partial y} = \frac{1}{\rho C_p}\left[\frac{\partial}{\partial y}\left(k\frac{\partial T}{\partial y} - \rho C_p\overline{v'T'}\right) + \frac{\partial}{\partial x}\left(k\frac{\partial T}{\partial x}\right)\right]. \tag{4}$$

The coefficients for Prandtl's mixing length, Boussinesq's eddy diffusivity, and a "turbulent Prandtl number" are defined, respectively, as

$$-\rho\overline{u'v'} \equiv \rho\epsilon_m\frac{\partial u}{\partial y}$$

$$-\rho C_p\overline{v'T'} \equiv \rho C_p\epsilon_h\frac{\partial T}{\partial y} \tag{5}$$

$$Pr_t \equiv \epsilon_m/\epsilon_h.$$

From the mixing length theory

$$\epsilon_m = l_m{}^2\frac{\partial u}{\partial y}, \tag{6}$$

where l_m is the mixing length. Near both surfaces, this model uses the modified mixing length theory of Van Driest[13] and Patankar and Spalding[14], which result in

$$\epsilon_m = \left(k_m y\left\{1 - \exp\left[\frac{-y(\tau\rho)^{1/2}}{\mu A^+}\right]\right\}\right)^2\frac{\partial u}{\partial y}, \tag{7}$$

where τ is the local shear stress, and where A^+ and k_m are empirical constants. Some distance away from the surfaces, it has been proposed by Escudier[15] that

$$\epsilon_m = (0.075\delta)^2\frac{\partial u}{\partial y} \tag{8}$$

be used whenever it is less than the expression (7). The parameter δ is taken to be the distance from the surface in question to the point where, (a) in the case of low flows, the time average velocity differs from minimum channel core velocity by one part in 10^4; or (b) in the case of high flows, the time average velocity differs from the maximum channel core velocity by one part in 10^4.

Eventually, as the flow becomes more fully developed, the boundary layers from both surfaces merge, after which the channel half-width is assumed to be the boundary layer thickness. Computations indicate that this assumption does not appear to significantly affect the thermal performance of the channel.

A study by Kays and Leung[10] on heat transfer in annular passages for fully developed turbulent flow stresses that "the turbulent flow problem is two orders of magnitude more complex than its laminar flow counterpart because Reynolds number and Prandtl number become parameters." Cebeci[16] has proposed a turbulent Prandtl number model expressed as

$$Pr_t = \frac{\epsilon_m}{\epsilon_h} = \frac{k_m}{k_h}\left\{\frac{1 - \exp[-y(\tau\rho)^{1/2}/\mu A^+]}{1 - \exp[-y(\tau\rho)^{1/2}/\mu B^+]}\right\}, \tag{9}$$

where close to the surfaces $Pr_t \approx (k_m/k_h)(B^+/A^+)$, and as y increases, $Pr_t \approx k_m/k_h$. However, in the attempt to improve the agreement between the computed values and the severely limited experimental data, a turbulent Prandtl number which gives slightly greater y dependence was desirable. A variable turbulent Prandtl number as defined by Meier and Rotta[18] and used by Cebeci[16] was adopted as follows

$$Pr_t = \left(\frac{k_m}{k_h}\left\{\frac{1 - \exp[-y(\tau_i\rho)^{1/2}/\mu A^+]}{1 - \exp[-y(\tau_i\rho Pr)^{1/2}/\mu B^+]}\right\}\right)^2, \tag{10}$$

where the shear stress τ_i is evaluated adjacent to the surface and is given by

$$\tau_i = -\mu \frac{du}{dy}\bigg|_s.$$

Various values of the constants k_m, k_h, A^+, and B^+ have been used to represent different experimental quantities of interest. The results of Kays and Leung[10] together with the data reviewed by Cebeci[16] were used to adjust parameters at high flow. Experimental and computational studies by Cheesewright[4], Mason and Seban[6], and Warner and Arpaci[4] on the single heated vertical plate provided a basis for evaluation and comparison of the constants at the lower flow rates. A series of preliminary computations appropriate for the range of expected flow rates led to the adoption of the following values: $k_m = 0.40$, $k_h = 0.43$, $B^+ = 33.8$, $A^+ = 26$. Equations (1)–(8) and (10) with the above constants form the framework of the model used in this computation.

The required expressions in dimensionless form are

$$\frac{\partial U}{\partial X} + \frac{\partial V}{\partial Y} = 0 \tag{11}$$

$$U\frac{\partial U}{\partial X} + V\frac{\partial U}{\partial Y} = \left(1 + \frac{\epsilon_m}{\nu}\right)\frac{\partial^2 U}{\partial Y^2} - \frac{\partial P}{\partial X} + \theta \tag{12}$$

where, near surfaces,

$$\frac{\epsilon_m}{\nu} = (k_m Y)^2 Gr\left\{1 - \exp\left[\frac{-Y\left(Gr\dfrac{\partial U}{\partial Y}\right)^{1/2}}{A}\right]\right\}^2\left|\frac{\partial U}{\partial Y}\right| \tag{13}$$

where τ is taken to be τ_i, and where

$$\frac{\epsilon_m}{\nu} = (0.075Y)^2 Gr\left|\frac{\partial U}{\partial Y}\right| \tag{14}$$

whenever it is less than eqn (14); and finally, eqn (4) becomes

$$U\frac{\partial \theta}{\partial X} + V\frac{\partial \theta}{\partial Y} = \frac{1}{Pr}\left(1 + \frac{Pr\epsilon_m}{Pr_t \nu}\right)\frac{\partial^2 \theta}{\partial Y^2}, \tag{15}$$

where the appropriate expression (13) or (14) is used for ϵ_m/ν and where (10) is used for Pr_t.

3. THE METHOD OF SOLUTION

The equations were solved using a forward-marching line-by-line implicit finite difference technique permitting iterations on each new line similar to that described in[1]. The equations are cast in matrix form as in[1] with the following modifications. The matrix elements of the energy and momentum equations are altered to include the quantities $[1 + (Pr/Pr_t)(\epsilon_m/\nu)]$ and $[1 + (\epsilon_m/\nu)]$ and are represented by AT and BT, respectively. The matrix elements in the energy equation take the following form

$$\begin{aligned} A_k &= -V^*_{j+1,k}(2\Delta Y)^{-1} - Pr^{-1}(\Delta Y)^{-2}(AT_{j,k-1} + AT_{j,k}) \\ B_k &= U^*_{j+1,k}(\Delta X)^{-1} + Pr^{-1}(\Delta Y)^{-2}(AT_{j,k-1} \\ &\quad + 2AT_{j,k} + AT_{j,k+1}) \\ C_k &= V^*_{j+1,k}(2\Delta Y)^{-1} - Pr^{-1}(\Delta Y)^{-2}(AT_{j,k} + AT_{j,k+1}). \end{aligned} \tag{17}$$

Those matrix elements modified by turbulence in the momentum equation become

$$\begin{aligned} E_k &= -V^*_{j+1,k}(2\Delta Y)^{-1} - (\Delta Y)^{-2}(BT_{j,k-1} + BT_{j,k}) \\ F_k &= U^*_{j+1,k}(\Delta X)^{-1} + (\Delta Y)^{-2}(BT_{j,k-1} \\ &\quad + 2BT_{j,k} + BT_{j,k+1}) \\ G_k &= V^*_{j+1,k}(2\Delta Y)^{-1} - (\Delta Y)^{-2}(BT_{j,k} + BT_{j,k+1}). \end{aligned} \tag{18}$$

The momentum equation is used to estimate the pressure gradient for the third and fourth iterations of row $j + 1$, which becomes

$$\begin{aligned} \left(\frac{dp}{dx}\right)_{j+1} &= -U^c_{j+1,m}(U^c_{j+1,m} - U_{j,m})(\Delta X)^{-1} \\ &\quad + [U^c_{j+1,m+1}(BT_{j,m} + BT_{j,m+1}) \\ &\quad - U^c_{j+1,m}(BT_{j,m-1} + 2BT_{j,m} + BT_{j,m+1}) \\ &\quad + U^c_{j+1,m-1}(BT_{j,m} + BT_{j,m-1})](\Delta Y)^{-2} \\ &\quad - V^c_{j+1,m}(U^c_{j+1,m+1} - U^c_{j+1,m-1})(2\Delta Y)^{-1} \\ &\quad + \theta_{j+1,m}. \end{aligned} \tag{19}$$

The calculation procedure is identical to that used in[1] except where discussed below. A uniform inlet velocity profile, the volumetric flow rate, the thermal boundary conditions, and the Grashof number are chosen. Laminar flow is assumed until the transition condition is reached. Should this condition be reached at row $j + 1$, the quantities represented by AT and BT are calculated using a U velocity profile which is an unweighted average of the converged profiles from the four rows $j, j - 1, j - 2, j - 3$. If the transitional condition is reached at the very first row, the inlet velocity profile is used. At row $j + 1$, the shear stress is computed as an unweighted average of the values calculated from the four rows j, $j - 1$, $j - 2$, and $j - 3$, using the smoothed U velocity profile. The values of AT and BT determined at row j are used in the calculation of θ_{j+1} and U_{j+1}. The averaging of the U velocity profile and the shear stress values tends to suppress oscillations which lead to computational instability. Typical grid sizes used for the various Grashof numbers are presented in the Appendix.

4. DISCUSSION OF RESULTS

The literature values k_m, k_h, A^+ and B^+ chosen for use in this model produce results which may be qualitatively compared to those of Cheesewright[3] when very low flow rates are assumed, and to those of Kays[17] when flow rates which approach those associated with forced convection characteristics are assumed.

At low flow rates, a quantitative comparison with the single plate results of Cheesewright is not possible due to differences in the problem geometry. However, for the case of nearly uncoupled channel flow, satisfactory qualitative agreement of velocity and temperature profiles is obtained for similar peak velocities and plate temperatures. The general appearance of typical velocity and temperature profiles is shown in Fig. 2.

At much higher flow rates, the characteristics of the velocity profile approach those of forced convection. The computed Nusselt numbers agree quite well with those found by Kays[17]. The similarities between the widely accepted turbulent forced flow velocity profiles and those computed by the present model at higher naturally induced flow rates can be observed in Fig. 3. In addition, at high flows, the limiting velocity and temperature profiles reached are similar to those observed in the case of forced flows (Fig. 4).

The model shows a high degree of continuity in velocity and temperature profile development, particularly when the plate temperatures are similar (Fig. 5). The discontinuities which appear are dealt with more fully in the ensuing discussions. It must be recognized that these undesirable features do not appreciably affect the collective details such as Nusselt numbers.

Computations were performed for a range of Grashof numbers and volumetric flow rates within the area bounded by points A–D of Fig. 6. A minimum of ten different volumetric flow rates were studied at each of the Grashof numbers 10^5, 10^6, 10^7, 10^8, and 10^9. Twenty relative plate temperatures were examined for each flow rate. Grashof numbers greater than 10^9 and less than 10^5 were considered to be outside the range of interest. Either large plate separations or greater temperature differences which result in Grashof numbers greater than 10^9 require major modifications of the assumptions made in the basic model. This limitation should pose no problem in foreseeable applications to architectural design.

At Grashof numbers lower than 10^5, the range of volumetric flow rates for which turbulence is predicted is greatly restricted. Therefore, the performance characteristics of laminar flow may be

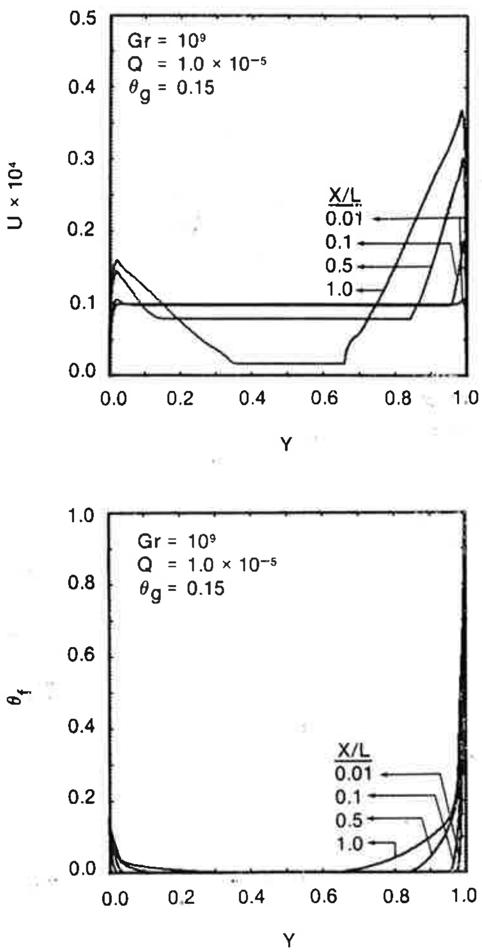

Fig. 2. General appearance of velocity and temperature profiles at low flow rates.

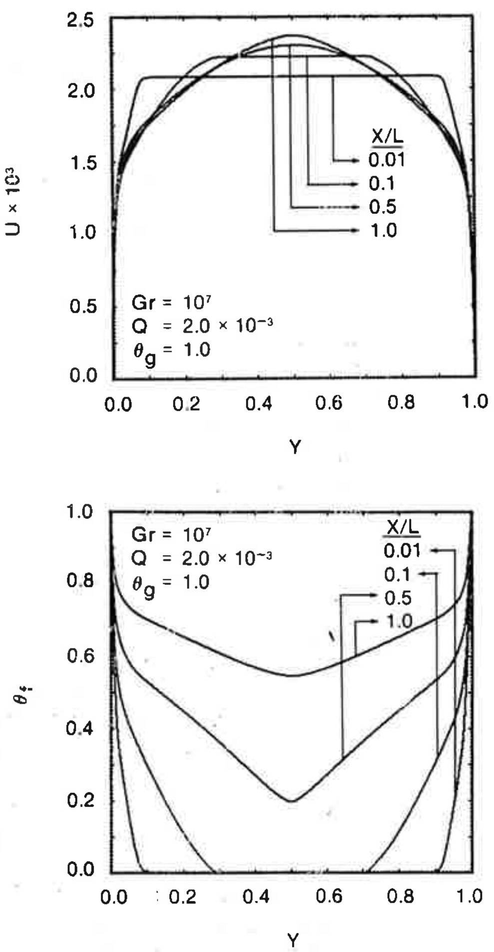

Fig. 3. General appearance of velocity and temperature profiles at high flow rates.

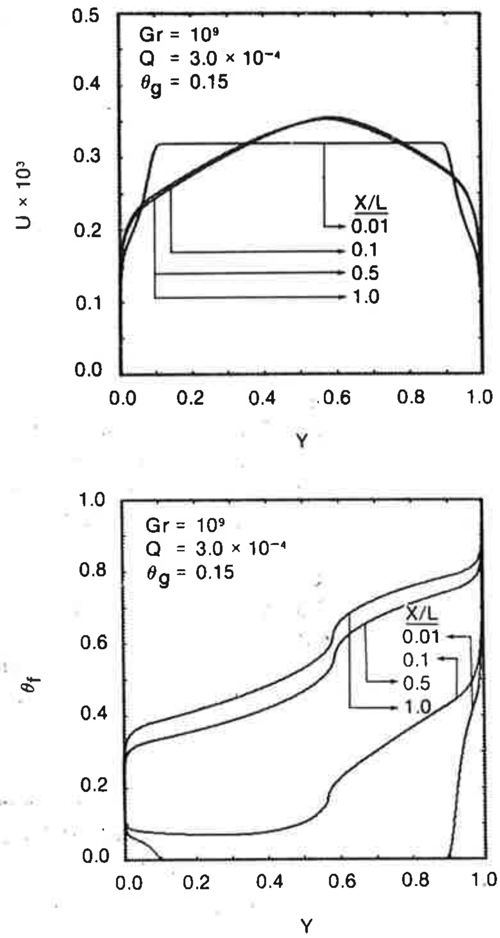

Fig. 4. General appearance of limiting velocity and temperature profiles at high flow rates with different plate temperatures.

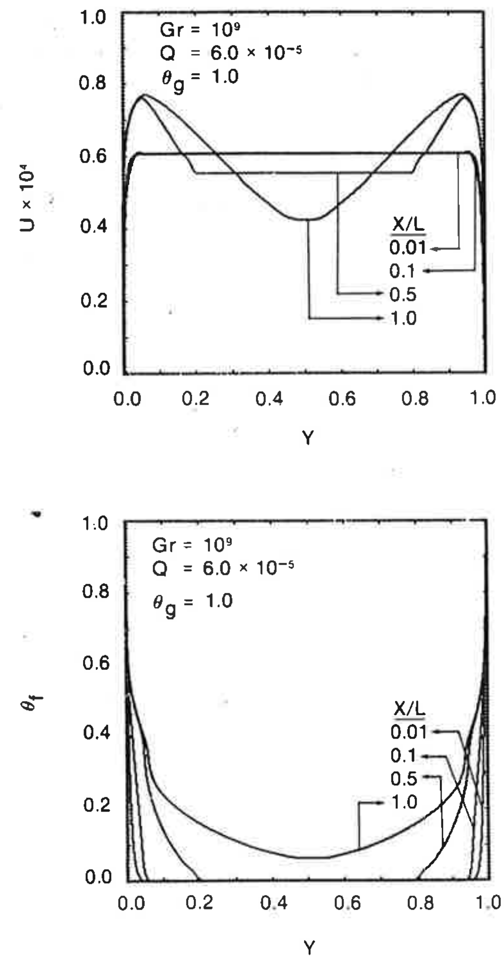

Fig. 5. General appearance of velocity and temperature profiles of equal plate temperatures.

adequate. The shaded area in Fig. 6 represents the approximate conditions for which this model predicts developing turbulence. On the basis of this model, conditions to be left of line *AG* result in completely laminar flow. Flow rates to the right of line *CD* appear to be physically unattainable within the basic assumptions of this model; therefore, no results are obtained for these conditions. For ease of interpretation we show the direction of constant fluid velocity, which is also the direction of constant temperature difference lines, by *EF*.

In this computational study, the effect of turbulence on characteristics such as the Nusselt numbers, velocity, and temperature profiles is examined. A systematic literature search has not revealed any experimental data to which the results of this computation may be directly compared. Therefore, these results are presented in some detail in order to discuss similarities with data which may be related, and to describe desirable and undesirable features of the turbulence model used here.

Figure 7 is representative of results obtained for a moderately high flow rate. Discontinuities in the *U*,

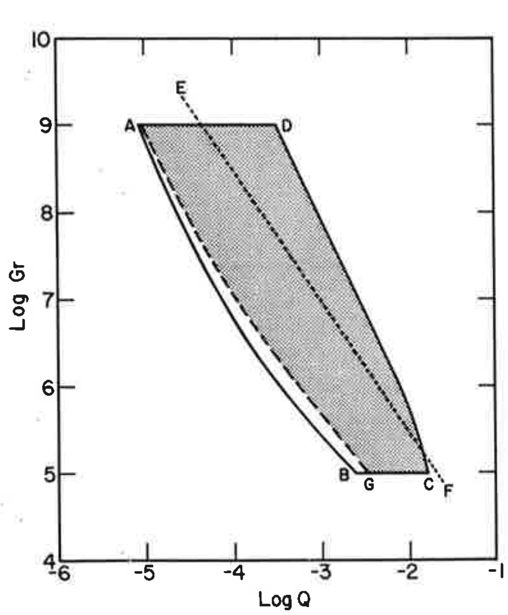

Fig. 6. Limits of flow rates and *Gr* numbers of the present study.

V and θ profiles which generally appear at approximately ten and ninety percent of the channel width are due to the change from the Van Driest to the Escudier approximation for ϵ_m and ϵ_h. Discontinuities which generally appear closer to the center of the channel, as for example in the temperature profile $\theta_g = 0.15$ near $Y = 0.6$, are due to the abrupt manner in which the boundary layer position is defined and turbulence is assumed to change with Y. These two undesirable details of the model just described could be greatly reduced. However, the lack of experimental data prevents an assessment of their importance to the final computed quantities of interest and brings into question the need to invest the additional effort to simply minimize their appearance. Turbulence which may develop adjacent to only one surface prior to, or to the exclusion of, the second can best be assimilated into a model after its importance and behavior is experimentally determined.

Noted below are characteristics of Fig. 7 which are useful in the comparison to profiles of other flow rates and geometries. The U, V and θ profiles for all θ_g at final elevation fractions of 0.01 and 0.10 show laminar flow behavior. Between elevation fractions of 0.10 and 0.50, the transition condition is reached and the U profile gradually assumes a more turbulent character. The lower θ_g values of 0.55 and 0.15 show that the U profile changes very little between elevation fractions of 0.5 and 1.0. This is indicated by much smaller maxima in the V velocity. The maximum in the U profile is positioned at considerably greater distance from the warmer surface than it is in

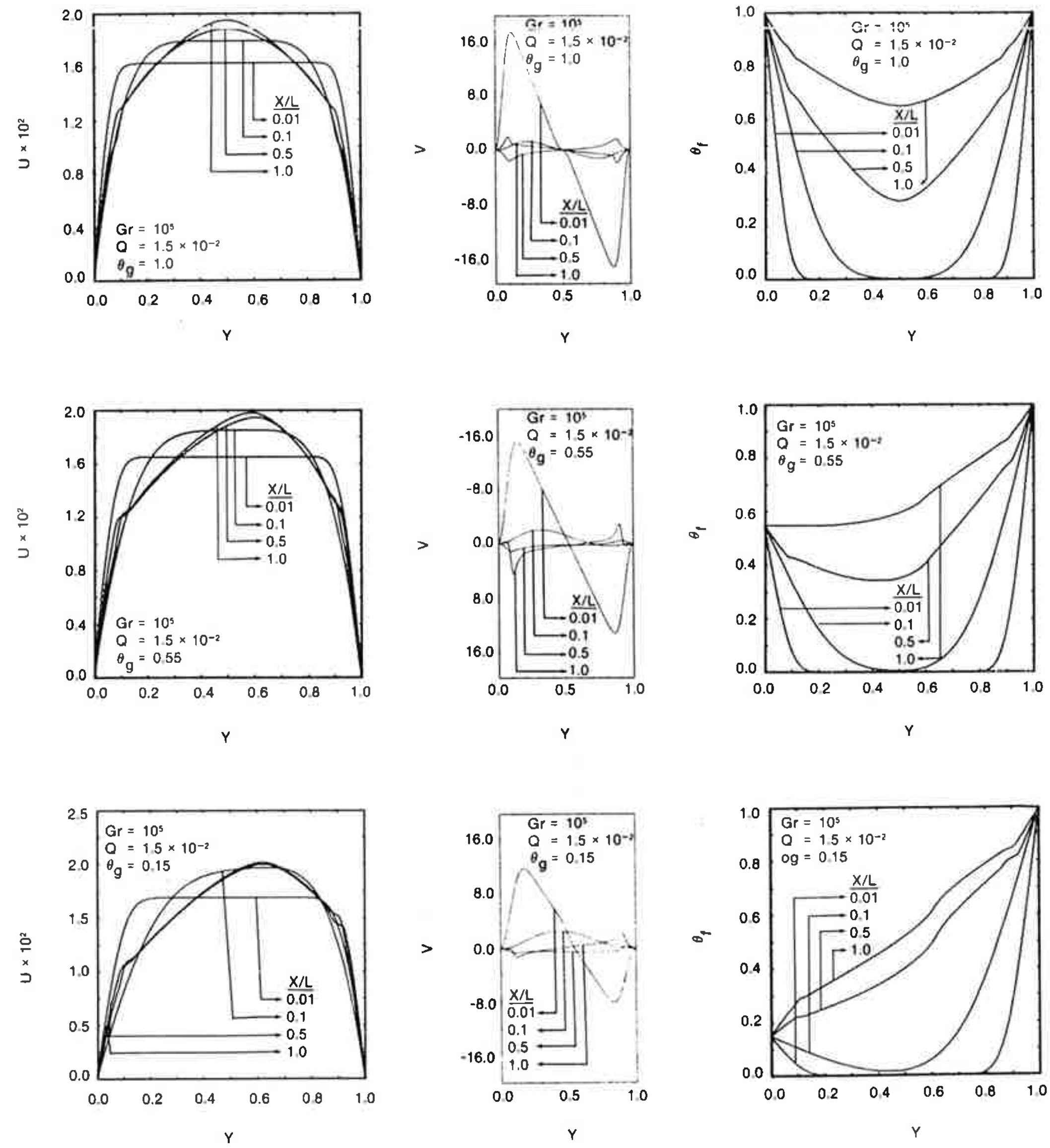

Fig. 7. U, V velocity and temperature profiles at four stages of development for three different glass temperatures, $Gr = 10^5$, $Q = 1.5 \times 10^{-2}$.

either the lower flow rate or laminar flow case. For $\theta_g = 0.15$, the rate at which the fluid acquires heat is large after turbulence is initiated, from 0.10 to 0.50 of the channel travel, but is greatly diminished thereafter. This rapid temperature rise is consistent with expectations of turbulent heat transfer.

Figure 8 represents an example of a high flow rate. Turbulence is initiated between elevation fractions of 0.01 and 0.10. Fluid which is relatively distant from the surfaces is noticeably heated soon after entry. The U velocity profile shows little development beyond $X/L = 0.50$ and is in close agreement with the 1/7 power law experimentally measured for forced flow.

A lower flow which shows turbulence early in the channel is shown in Fig. 9. The discontinuities of the model are quite evident in the V profiles. Discontinuities due to the boundary layer are less noticeable for the lower flows in which the U velocity profile shows a minimum in the central region and become almost non-existent if the fluid is symmetrically heated.

Figure 10 shows how the development of turbulence in a moderately high flow condition with one relatively cool plate affects the local Nusselt numbers and the pressure defect. Referring to the pressure defect behavior vs fraction of wall height traveled, it is noticed that the transition point is reached at approximately 12 percent of the wall height as is evidenced by a discontinuity in the pressure defect caused by a rapid change in velocity and temperature profiles.

The warmer surface Nusselt number and the total

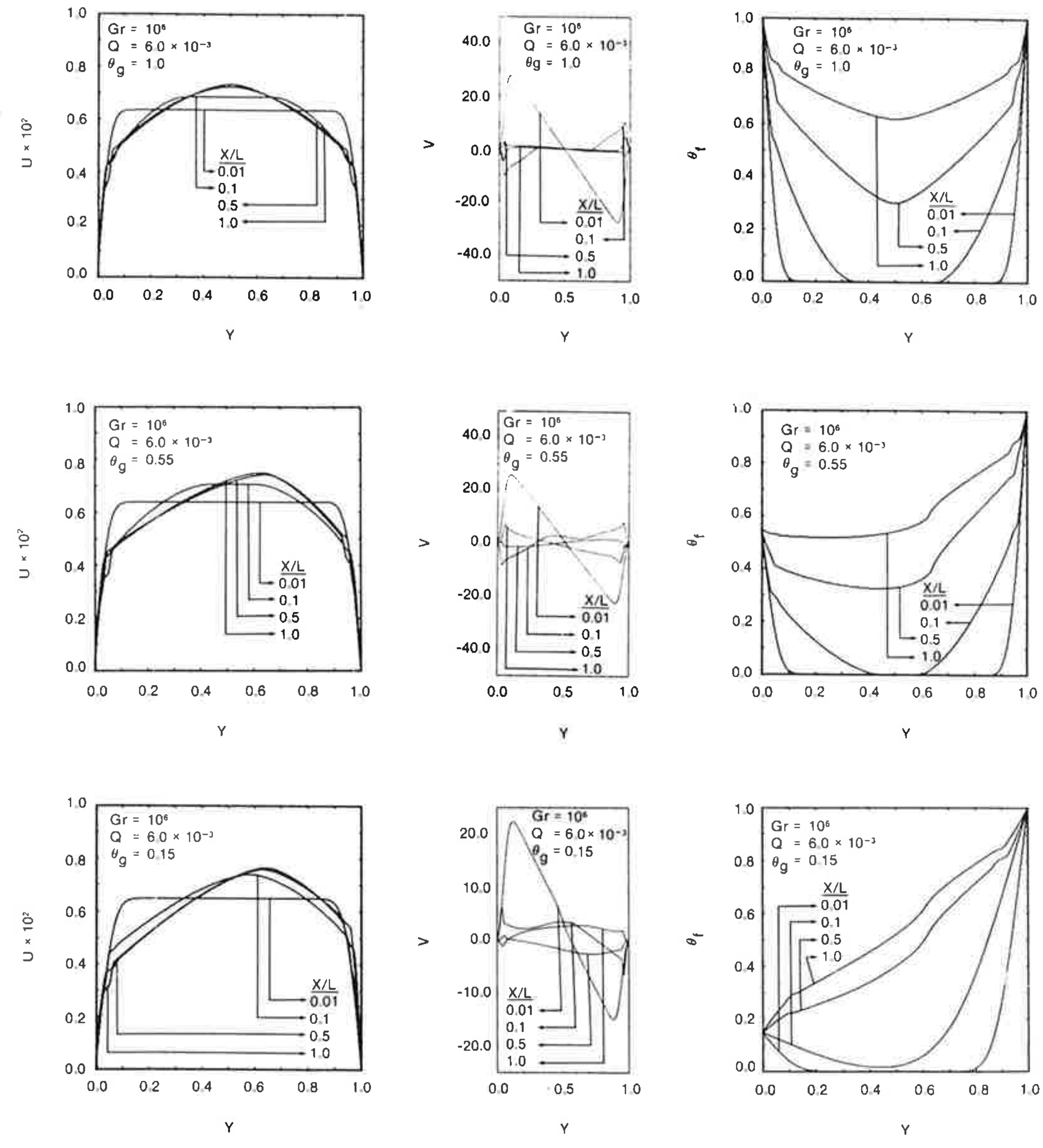

Fig. 8. U, V velocity and temperature profiles at four stages of development for three different glass temperatures, $Gr = 10^6$, $Q = 6.0 \times 10^{-3}$.

Nusselt number are plotted separately from that of the cooler surface. The value of the total Nusselt number is greater than that of the warmer surfaces until heat is lost by the fluid to the cooler surface; this is indicated by a change in sign of the Nusselt number of the cooler surface. A sudden rise in the values of the Nusselt numbers at the transition point is consistent with the developing U, V and θ profiles which are included in Fig. 7 for this particular case. It is also evident from Fig. 7 that the parabolic development in U and the θ profile characteristic of laminar development are altered after 10 percent of the plate height is traveled. In Fig. 10, the oscillations which follow the sudden rise in Nusselt numbers are computational in nature. These oscillations may be due, in part, to the incremental nature of the boundary layer thickness.

5. CORRELATIONS

Least squares techniques have been used to develop several correlations which provide an estimate of important quantities of interest. Attempts were not made to generate correlations for parameters such as the pressure defect, the total Nusselt numbers, and the total heat flux along the flow axis. The expressions which were developed are algebraically lengthier than those developed for the laminar flow study[1] due to the presence of turbulent flow development, and the additional dimension required by the Grashof number.

The induced flow rate as a function of the total height, the relative plate temperatures, and the Grashof number may be estimated from

$$Q = 10^{-(C+D|\log L|^{z})} \tag{20}$$

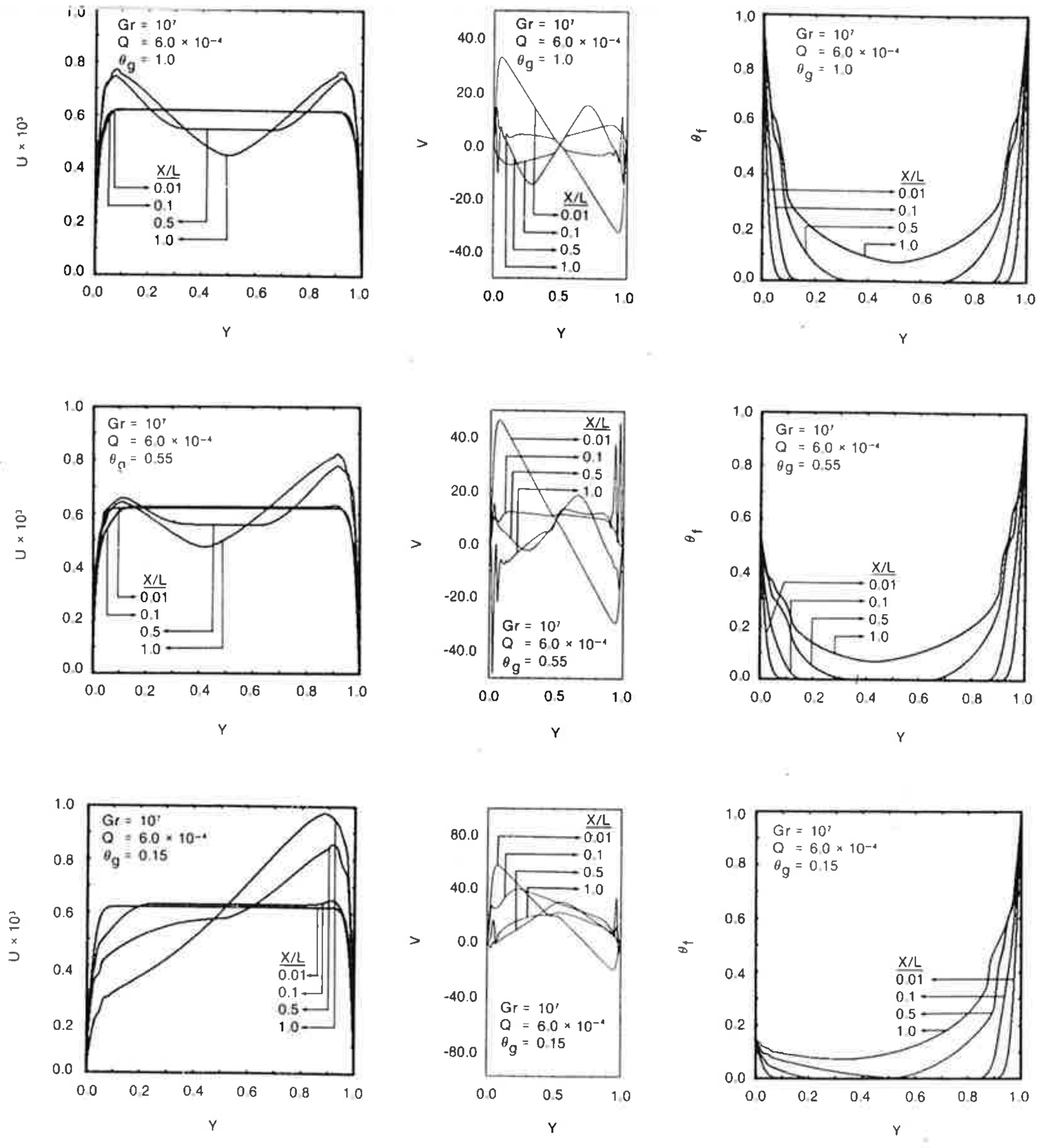

Fig. 9. U, V velocity and temperature profiles at four stages of development for three different glass temperatures, $Gr = 10^7$, $Q = 6.0 \times 10^{-4}$.

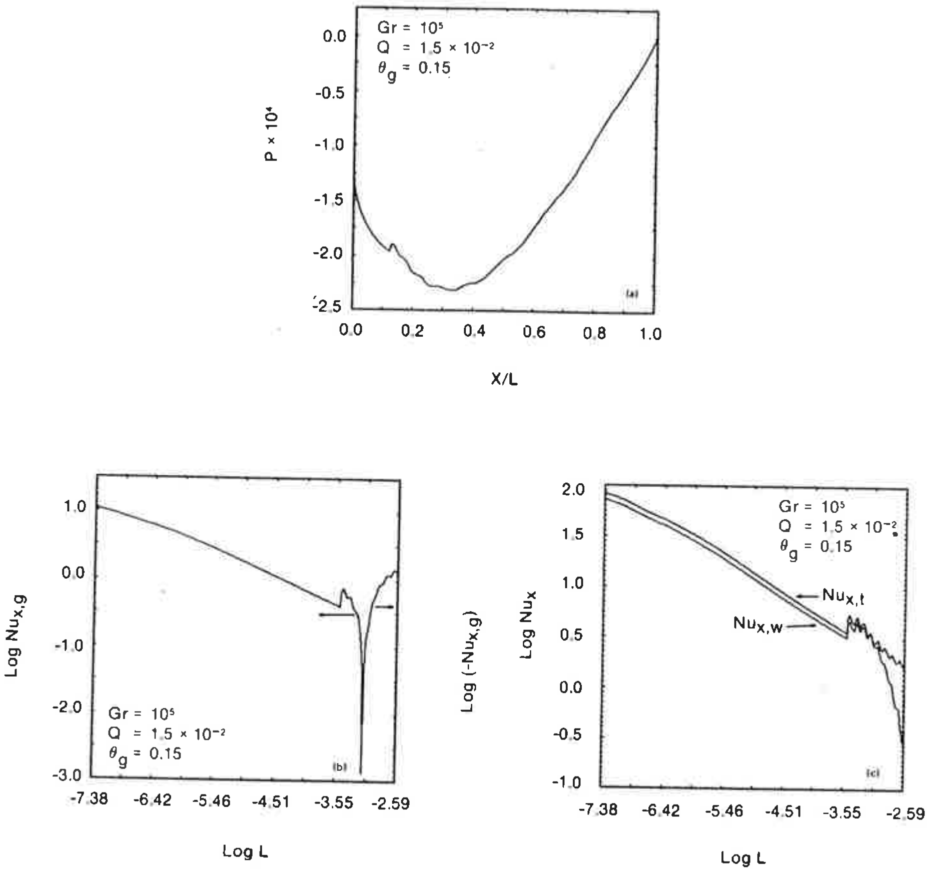

Fig. 10. The characteristic behavior of (a) pressure defects, (b) Nusselt number of glass, (c) Nusselt number of wall and total Nusselt number as a function of height.

where

$$C = E\theta_g^{\ \beta}$$

$$\alpha = 0.260 + 1.940(\log Gr - 4)^{1/2}$$

$$\beta = -1.134(\log Gr)^{-1.768}$$

$$D = 10^{(1.931 - 0.6444 \log Gr)}$$

$$E = -0.7628 + 0.3984 \log Gr.$$

An estimate of the induced flow rate may be useful in instances which require the plates to be of a given height and spacing.

The total height as a function of the relative plate temperatures, Grashof number, and flow rate may be estimated from

$$L = 10^{C\theta_g^\alpha} \tag{21}$$

where

$$C = D + E|\log Q|^{-1}$$

$$\alpha = F \exp(B|\log Q|^{-10})$$

$$B = 10^{[-4.210 + 1.637 \log Gr - 0.06040(\log Gr)^2]}$$

$$D = -5.494 + 0.03780 \log Gr - 0.08886(\log Gr)^2$$

$$E = 10.36 - 2.361 \log Gr + 0.3936(\log Gr)^2$$

$$F = 10^{[0.9283 - 0.6545 \log Gr + 0.03477(\log Gr)^2]}.$$

The rate at which heat is removed by the fluid at the exit in terms of the volumetric flow rate, the Grashof number, and relative temperatures can be estimated by

$$H_L = 10^{[a + b(\log Q + 5.1)^\alpha]} \tag{22}$$

where

$$a = D(\theta_g + F)^\gamma$$

$$b = E(\theta_g + G)^\beta$$

$$\alpha = P(\theta_g - 0.050)^\delta$$

$$\beta = -12.01068 + 3.848347 \log Gr - 0.4237468(\log Gr)^2 + 0.01593455(\log Gr)^3$$

$$\gamma = -0.4913 + 0.09517 \log Gr - 1.346 \times 10^{-3} \times (\log Gr)^2 - 5.800 \times 10^{-4}(\log Gr)^3$$

$$\delta = 28.65 \exp[-1.715(\log Gr)^{0.60}]$$

$$D = 7.137 - 4.841 \log Gr + 0.7525(\log Gr)^2 - 0.04398(\log Gr)^3$$

$$E = -2.807838 + 1.554883 \log Gr - 0.2897646(\log Gr)^2 + 0.01846012(\log Gr)^3$$

$$F = -0.11478 + 4.531 \times 10^{-4} Gr^{0.4327}$$

$$G = -157.9611 + 334.1465(\log Gr)^{0.2} - 235.5351(\log Gr)^{0.4} + 55.32535(\log Gr)^{0.6}$$

$$P = 5.938 - 0.4465 \log Gr - 5.503 \times 10^{-3}(\log Gr)^2.$$

The development of a correlation for the total average Nusselt number was found to be time-consuming. Its value, however, may be estimated from the correlated values of H_L and L by using the relationship

$$\overline{Nu_t} = H_L Pr / L. \tag{23}$$

6. ERROR ANALYSIS

A few characteristics of the correlations described in the previous section and the computed values of the important quantities are comparatively shown in Fig. 11.

An exhaustive comparison has been made between the correlated and computed values of all the quantities of interest over the entire range of the study. The absolute difference between the computed results and the correlated predictions can be expressed as a per cent error. Figure 11(d) is a plot of the percentage of total computed data vs the per cent error and indicates the degree of confidence with which the correlations predict the computed data. Figure 11(d) shows that the correlations which were developed estimate 94 per cent of the computed data to within 20 per cent error.

7. CONCLUSION†

A line-by-line forward marching implicit difference method has been used in the study of free convective turbulent flow between parallel vertical plates of different temperatures. A mixing length model was adopted which uses a variable turbulent Prandtl num-

†At the time development of this work was in progress, the authors could not find any related experimental work to compare with the correlations. During the last four years, several experiments have dealt with this subject, one of which is Akbarzadeh *et al.*[19]. These authors have compared their experimental results with the predictions of numercial models.

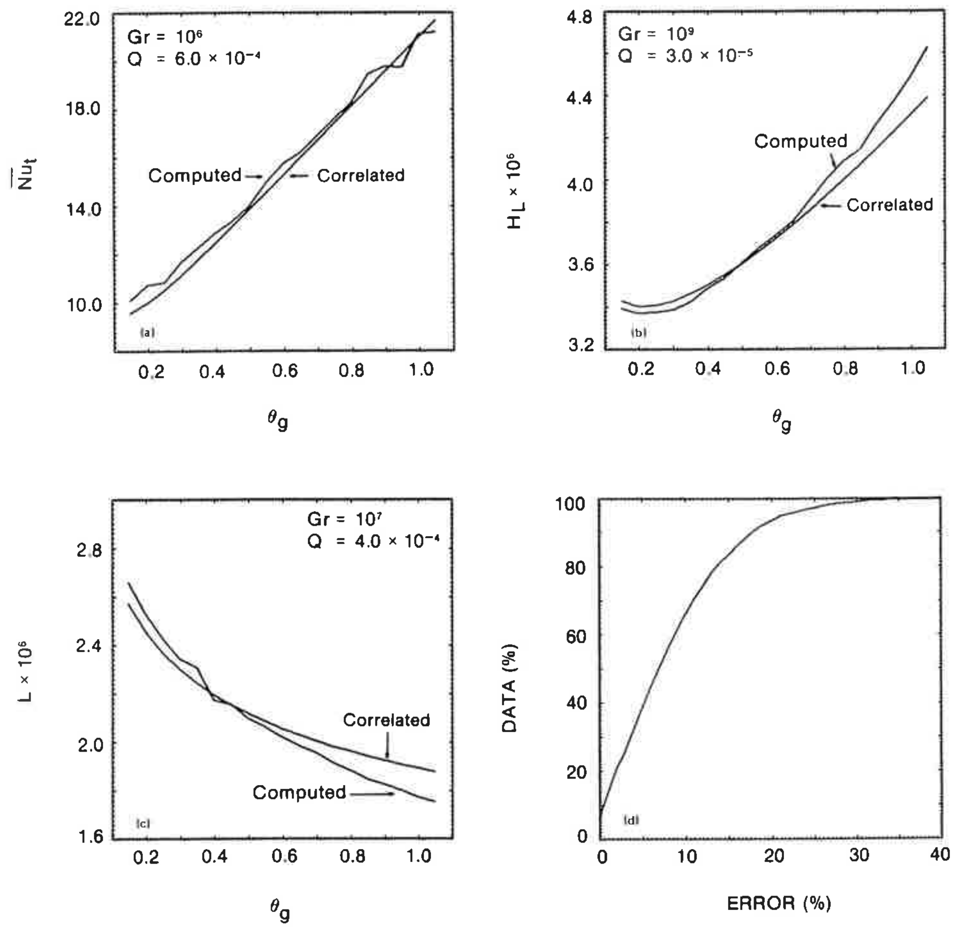

Fig. 11. Comparison of computed and correlated results for (a) total average Nusselt number; (b) total heat extracted, and (c) total channel height as a function of glass temperature. (d) is the cumulative error encountered in correlations.

ber and values of the empirical constants commonly found in the literature.

A wide range of flow rates and plate spacings was investigated. The model indicated that if the dimensionless flow is less than $10^{-(\log Gr-1.16)/1.54}$, the flow is probably laminar and the correlations which were developed for laminar flow in an earlier study should be applicable. The model also indicated that if the dimensionless flow is greater than $10^{-(\log Gr-0.76)/2.35}$ the magnitude of the flow seemed to be physically unattainable.

Results were obtained for a minimum of ten different volumetric flow rates within the bounds noted above, each with twenty relative plate temperatures at each of the Grashof numbers 10^5, 10^6, 10^7, 10^8, and 10^9.

Three correlations were developed from which important overall performance characteristics of the wall may be estimated. An exhaustive comparison shows that the correlations estimate more than 90 per cent of the computed results to within 20 per cent error.

Acknowledgements—This work has been supported by the Solar Heating and Cooling Research and Development Branch, Office of Conservation and Solar Applications, U.S. Department of Energy, under Contract No. W-7405-ENG-48. We wish to express sincere thanks for the helpful discussions with Prof. R. A. Seban, Department of Mechanical Engineering, University of California at Berkeley. This study was performed as part of the Passive Solar Analysis Project in the Solar Program administered by R. Kammerud at Lawrence Berkeley Laboratory.

NOMENCLATURE

A empirical constant
AT $= 1 + [(Pr/Pr_t)(\epsilon_m/\nu)]$
B empirical constant
BT $= 1 + \epsilon_m/\nu$
b width of channel (plate separation), m
β coefficient of volumetric thermal expansion, K^{-1}
C_p specific heat of fluid, $kJ\,kg^{-1}\,K^{-1}$
δ boundary layer thickness
ϵ_h thermal eddy diffusivity
ϵ_m momentum eddy diffusivity
g gravitational acceleration, 9.801 $m\,s^{-2}$
Gr Grashof number, $= g\beta(T_m - T_0)b^3\nu^{-2}$
Gr_x Grashof number based on the elevation of channel, $= g\beta(T_m - T_0)x^3\nu^{-2}$
$\bar{h}$ average heat transfer coefficient, $kW\,m^{-2}\,K^{-1}$
$\dot{h}$ rate of heat absorption per width of wall, $kW\,m^{-1}$
H_L dimensionless rate of heat absorption by fluid at channel exit
k thermal conductivity of fluid, $kW\,m^{-1}\,K^{-1}$
k_h empirical constant
k_m empirical constant
l length of channel, m
l_m mixing length
L dimensionless height of channel
ν kinematic viscosity, m^2s^{-1}
$\overline{Nu_t}$ total average Nusselt number
$Nu_{x,i}$ local Nusselt number, $i = g, w, t$
p pressure at elevation x, $kg\,m^{-2}$
p_∞ ambient pressure at elevation x, $kg\,m^{-2}$
P dimensionless pressure defect, $b^2(p - p_\infty)\nu^{-2}Gr^{-2}\rho^{-1}$
Pr Prandtl number
Pr_t turbulent Prandtl number, ϵ_m/ϵ_h
q volume flow rate, m^2s^{-1}
Q dimensionless volume flow rate
Re Reynolds number
ρ fluid density, $kg\,m^{-3}$
T temperature, K
T' temperature fluctuation
θ dimensionless temperature, $(T - T_0)/(T_m - T_0)$
T_m reference temperature, defined as the temperature of the warmer surface of the channel, K
τ local shear stress
τ_i shear stress at surface i
u fluid velocity, x-direction, $m\,s^{-1}$
U dimensionless fluid velocity, X-direction
u' u velocity fluctuation
v fluid velocity, y-direction $m\,s^{-1}$
V dimensionless fluid velocity, Y-direction
v' v velocity fluctuation
x, y Cartesian coordinates, m
X, Y dimensionless Cartesian coordinates

Subscripts

f fluid
g glass
m grid point at which maximum U velocity occurs
0 inlet
t total
w wall
x elevation

The following relations exist

$$u = UvGrb^{-1}$$
$$l = LGrb$$
$$v = Vvb^{-1}$$
$$y = Yb$$
$$T = \theta(T_m - T_0) + T_0$$
$$(p - p_\infty) = P\rho v^2Gr^2b^{-2}$$
$$Gr = g\beta(T_m - T_0)b^3v^{-2}$$
$$\bar{h} = \overline{Nu_t}kb^{-1}$$
$$\dot{h} = H_LvGr(T_m - T_0)\rho C_p$$
$$H_L = L\overline{Nu_t}Pr^{-1}$$
$$q = QvGr$$

REFERENCES

1. H. Akbari and T. R. Borgers, Free convective laminar flow within the trombe wall channel. *Solar Energy* **22**:2 (1979).
2. E. R. G. Eckert and T. W. Jackson, Analysis of turbulent free-convection boundary layer on a flat plate. *NACA TN* 1015 (1951).
3. R. Cheesewright, Turbulent natural convection from a vertical plane surface. *J. Heat Trans.* **90C**, 1 (1968).
4. C. Y. Warner and V. S. Arpaci, An experimental investigation of turbulent natural convection in air at low pressure along a vertical heated plate. *Int. J. Heat Mass Trans.* **11**, 397 (1968).
5. H. Kato, N. Nishiwaki and M. Hiruta, On the turbulent heat transfer by free convection from a vertical plate. *Int. J. Heat Mass Trans.* **11**, 1117 (1968).
6. H. B. Mason and R. A. Seban, Numerical predictions for turbulent free convection from vertical surfaces. *Int. J. Heat Mass Trans.* **17**, 1329 (1974).
7. T. Cebeci and A. Khattab, Prediction of turbulent free convective heat transfer from a vertical flat plate. *J. Heat Trans.* **97**, 469 (1975).
8. C. C. Vliet and C. K. Liu, An experimental study of turbulent natural convection boundary layers. *J. Heat Trans.* **91**, 517 (1969).
9. A. P. Hutton and A. Quermby, The effect of axially varying and unsymmetrical boundary conditions on heat transfer with turbulent flow between parallel plates. *Int. J. Heat Mass Trans.* **6**, 903 (1963).

10. W. M. Kays and E. Y. Leung, Heat transfer in annual passages—hydrodynamically developed turbulent flow with arbitrarily prescribed heat flux. *Int. J. Heat Mass Trans.* **6**, 537 (1963).
11. S. H. Lock and F. J. Trotter, Observations on the structure of a turbulent free convection boundary layer. *Int. J. Heat Mass Trans.* **11**, 1225 (1968).
12. F. Godaux and B. Gebhart, An experimental study of the transition of natural convection flow adjacent to a vertical surface. *Int. J. Heat Mass Trans.* **17**, 93 (1974).
13. E. R. Van Driest, On turbulent flow near a wall. *J. Aero. Sci.* **23**, 1007 (1956).
14. S. V. Patankar and D. B. Spalding, *Heat and Mass Transfer in Boundary Layers*, 2nd Edn. Intertext Books, London (1970).
15. M. P. Escudier, The distribution of mixing length in turbulent flows near walls. Imperial College, Heat Transfer Section. *Rep. TWF/TN/*1 (1966).
16. T. Cebeci, A model for eddy conductivity and turbulent Prandtl number. *J. Heat Trans.* **95**, 227 (1973).
17. W. M. Kays, *Convective Heat and Mass Transfer*. McGraw-Hill, New York (1966).
18. H. U. Meier and J. G. Rotta, Experimental and theoretical investigations of temperature distributions in supersonic boundary layers. *AIAA Paper No.* 70-744, *AIAA 3rd Fluid Plasma Dyn. Conf.*, Los Angeles, California (1970).
19. A. Akbarzadeh, W. W. S. Chaters and D. A. Lesslie, Thermocirculation characteristics of a trombe wall passive test cell. *Solar Energy* **28**, 361 (1982).

APPENDIX

With $\Delta Y = 2.5 \times 10^{-3}$, the initial X grid dimension and multiplier chosen for each computation varied with the Grashof number and the flow rate. Representatives values are shown in Table 1 for the range of Grashof numbers studied.

Table 1. Typical grid sizes and multipliers

GR	Q	ΔX	M
10^5	0.015	0.6×10^{-7}	1.03
10^5	0.0025	0.1×10^{-7}	1.03
10^7	0.003	0.4×10^{-7}	1.02
10^7	0.00008	0.75×10^{-9}	1.02
10^9	0.0004	0.20×10^{-8}	1.02
10^9	0.00001	0.60×10^{-10}	1.008